DAVID G. TILLEY and DAVID J. YEMC

WAVE DOMAIN PROCESSING OF SYNTHETIC APERTURE RADAR SIGNALS

Synthetic aperture radar (SAR) images are being created with new Fourier wavenumber domain algorithms that are more accurate than the traditional range-Doppler algorithm. A geometric distortion called range migration occurs when SAR images are formed under the assumption that the remote sensor is strictly side-looking. This article reviews the wave domain algorithms developed in Canada and Germany; our purpose is to clarify their common approach to creating more accurate SAR images using chirp scaling methods. Virtual SAR modeling software is being developed at APL to test new image processing methods, including new wave domain algorithms, and to evaluate geometric accuracies.

INTRODUCTION

Synthetic aperture radar (SAR) signal processing is concerned with the matched two-dimensional filtering of pulsed radar waveforms, which are transmitted and received by a remote sensor moving along its flight trajectory, to compute an image of the terrain that reflects the illumination back from the ground track. Wave domain algorithms are a class of new computer processing techniques that accomplish this task. The traditional range-Doppler algorithm applied filters (one-dimensional) to form the down-range and along-track image coordinates independently. The new chirp scaling method recognizes that range time delay and Doppler frequency shift are linked by the quadratic phase modulation applied to SAR pulses (i.e., a chirp with frequency increasing during the pulse time). The method uses this relationship in the design of two-dimensional filters that reduce geometric errors. In this article, the Data Processing Sequence section describes our computer processing procedures and can be skimmed lightly by the reader not interested in the mathematical details.

As a result of previous interdepartmental research at APL, digital terrain elevation data for the mountains near Huntsville, Alabama, were used to develop methods for correcting geometric and radiometric layover distortions of SAR imagery.[1] Topographic applications require use of these analytic image processing methods; they also require the development of interferometric capabilities along track and new procedures for processing SAR signals acquired at high squint angles.

Recently, new interferometer and spotlight mode applications of SAR have highlighted geometric and phase errors that are fundamental to the range-Doppler algorithm. The traditional assumption of a side-looking geometry is crucial to the range-Doppler algorithm. The algorithm is not accurate, however, when the SAR perspective must be shifted to large squint angles (e.g., 30° forward or backward, as well as to the side) in relation to the remote sensor location. In spotlight mode, the SAR focus is fixed on a target passing below, and an image of surrounding terrain is sacrificed to obtain a high-resolution image of a small scene. Similarly, a SAR operating as an interferometer measures the terrain elevation from signal phase differences observed simultaneously from different antennas along the trajectory of the remote sensor. A problem called range migration occurs in this and other wide-swath SAR imaging applications where large squint angles are needed to adequately focus targets separated by large look angles (30–60°) relative to nadir. In the past, satellite SAR system design with the range-Doppler algorithm has limited geometric distortions to less than 1% by processing narrow swaths with look angles between 20 and 25° and squint angles less than 10°.

Recent SAR signal data were acquired from the European Remote Sensing satellite ERS-1 and were processed to form scenes of the Chesapeake Bay, which were then compared with SAR scenes from other satellites. The objective was to produce SAR imagery from raw radar data using a new wave domain process. We sought to demonstrate a capability for testing the SAR imaging algorithms that have been proposed for satellite and airborne platforms of interest to the Navy, Army, and Air Force.

Surveillance of Coastal Environments

The Atlantic Coast of the United States has been studied with SAR since the first images from Seasat in 1978 revealed unique environmental signatures of atmospheric winds, bottom topography, geostrophic currents, internal wave solitons, and surface wave fields. A 1984 issue of this *Digest* presented examples of each of these environmental systems, demonstrating the Laboratory's early interest in SAR image processing.[2] Current rips and shoaling off Nantucket Island, wind roughening of the Chesapeake Bay, and dispersion of surface waves by the Gulf Stream all have been studied with SAR imagery.[3–5]

An atmospheric front was located over the Chesapeake Bay near the Bay Bridge at Kent Island on 9 May 1992. The SAR backscatter from the Bay was uniformly high

north of the front, indicating wind speeds sufficient to roughen the water surface at the 5-cm wavelength of the C-band ERS-1 remote sensor. Below the front, the Bay was dark except for several parallel striations, possibly caused by an increase in the microscale breaking of short wind-generated waves. The spatial pattern, or signature, of the wind stress may have been caused by air–sea temperature differences that modulated the buoyancy of the horizontal air flow. Nearly coincident advanced very high resolution radiometer (AVHRR) imagery and surface weather maps from the National Oceanographic and Atmospheric Administration (NOAA) were used to support these interpretations of the atmospheric signature that appeared in the ERS-1 SAR image of the Chesapeake Bay.

Guidance of Precision Strike Weapons

Precision strike weapons are key components of the Navy's arsenal, and since the closing of the Cold War, the emphasis has shifted from the open ocean to littoral seas.[6] Recent combat engagements by U.S. forces show that the precise delivery of weapons to fixed and mobile targets is a high priority. During the Desert Storm conflict, successful precision strikes were heralded in the mass media, and civilian casualties were reported when weapon guidance systems failed. Although the utility of particular guidance and surveillance systems was much debated, the successful outcome of the conflict was clearly hastened by the advanced technologies in use throughout the military.

Among the many available technologies for surveillance and precision guidance, SAR is an increasingly attractive choice. Because SAR systems are not obstructed by weather and require no external sources of light or heat, they are particularly desirable in the combat arena. Microwaves illuminate the scene and computer processing converts radar signals into images. The challenges for military SAR technology are to move toward higher resolution with geometric accuracy, to improve automatic target recognition, and to keep development costs low.

High-performance SAR remote sensors are being proposed for new guidance systems, and experimental prototypes are being constructed.[7] Unfortunately, development is costly, and flight tests may only partially resolve performance issues. The virtual SAR concept (Fig. 1) is a cost-efficient alternative for visualizing littoral regions by modeling platform trajectory, simulating microwave backscatter, and processing radar signals to create images of targets against background clutter. Performance can be analyzed with a computer model of the entire SAR–environment system. Virtual SAR can reduce development time and expense, allowing SAR technology to be economically incorporated throughout the military.

Remote Sensing for Atmospheric and Ocean Physics

Microwave scatterometers and imaging radars respond to the very-short-scale, wind-generated waves that are modulated by longer waves, subsurface currents, and bottom topography. Remote sensing of the ocean with

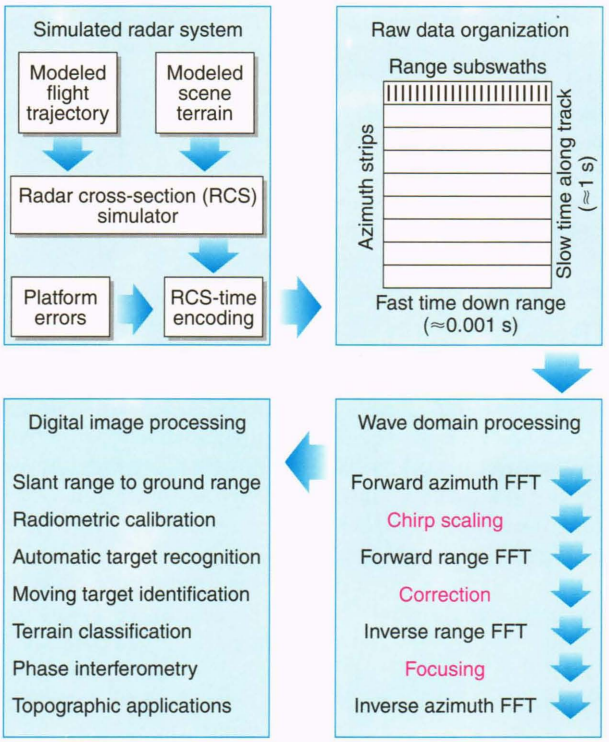

Figure 1. The concept of virtual SAR allows for the simulation of radar signal data that can be processed into images of terrain against backgrounds of clutter. Actual SAR data from the ERS-1 satellite were used to develop Matlab computer software for the wave domain processing block at the lower right (FFT = fast Fourier transform).

SAR is unique in that it employs the Doppler frequency shift at surface scattering sites to synthesize the along-track image coordinate. Hence, SAR along-track resolution is influenced by the wave field and its Doppler velocity statistics, which ocean physicists use to describe the hydrodynamic transfer of wave energy from shorter to longer waves. Detailed case studies[8] of the SAR modulation transfer function, describing remote sensing of long ocean waves with a C-band radar, require an understanding of atmospheric and ocean physics. Once SAR's measurement capabilities are well defined, the technology can be useful in monitoring environmental processes that influence the ocean surface wave field.

Surface wave fields are important indicators of wind stress, bottom friction, internal waves in the subsurface boundary layer, and large-scale currents. For example, SAR observations of the refraction and dispersion of waves crossing the Gulf Stream have been used to estimate the current velocity profile.[4] Wind-generated waves also influence the exchange of heat, mass, and momentum at the air–sea interface. Recently, a research vessel from Ukraine made *in situ* measurements of winds, temperatures, and currents near the Gulf Stream in support of SAR and AVHRR estimates of the stream's location.[9] The SAR image modulations appear well explained by the combination of an equilibrium model of wind–wave growth limited by breaking and an atmospheric stability model driven by the air–sea temperature difference.

SAR SIGNAL PROCESSING METHODS

Historically, SAR image processing has evolved from real aperture radar processing in one dimension down range to include Doppler frequency processing for improving resolution along the flight track. Pulse compression algorithms using matched filters in the Fourier frequency domain were developed in the 1950s to improve radar range resolution for single radar chirps modulated in frequency over the pulse duration. In the 1960s it was recognized that similar Doppler compression algorithms using matched filters in the Fourier frequency domain could be developed to improve radar resolution along track if pulses were repeated periodically. Hence, SAR image processing developed as two sequential operations, the rectangular range-Doppler algorithm,[10] in which Fourier frequency filters are applied independently on short time scales (to improve radar resolution down range) and then on long time scales (to improve radar resolution along track).

Wave domain SAR processing techniques offer an alternative to the range-Doppler algorithm. This idea was the theme of the session "SAR Wave Domain Processors" at the 1992 International Geoscience and Remote Sensing Symposium in Houston, Texas. At the symposium, Doppler frequency correlations of radar signal data were reported to be more accurate and efficient when range migration was anticipated during aperture synthesis and compensated in the Fourier wavenumber domain before pulse compression. To address the changing perspective of the remote sensor as it passed over points on the Earth, phase shift functions had been applied to signal data in the appropriate time and frequency domains. Hence, the effects of spherical geometry on resolving two orthogonal SAR coordinates, slant range r and azimuth a, had been approximated and accommodated. A wave domain method for addressing range curvature has been developed independently at the Canada Centre for Remote Sensing (CCRS) and at the German Aerospace Research Establishment (DLR). These chirp scaling algorithms[11,12] appear to be quite general in addressing high-squint and wide-swath SAR imaging geometries. In keeping our expertise in SAR image processing current, APL has derived chirp scaling algorithms from the CCRS and DLR approach using the notation and optical SAR model[3] developed for the NASA Seasat and space shuttle geometries.

Background

The linear SAR model[13] of signal frequency modulation by the Doppler effect is not invariant with respect to radar ranging measurements made at the same time. Range curvature, range walk, and range migration are all terms used to describe range-Doppler measurement errors that arise when the SAR geometry changes during the time required to transmit and receive several hundred repetitions of the pulsed radar waveform.

In developing a range-Doppler SAR processor[14] at APL, geometric range curvature errors were shown to be partially correctable. However, database interpolation addressing linear range walk added to the computational burden, and the residual range migration was found to complicate and compromise Doppler data compression. The traditional assumption that a side-looking SAR transmits in a direction perpendicular to its travel is not accurate over the entire synthetic aperture created along the flight path. This "Doppler aperture"[3] is shown in Fig. 2, which depicts the SAR geometry for broadcasting radar pulses periodically over a long interval of time τ, on the order of 1 s, from a platform moving with velocity V, to define the azimuth coordinate, $a = V\tau$. The individual pulses travel a different distance R down range before spreading out on the ground over a short interval of time t, on the order of 1 ms, to define the Huygen aperture and the slant range coordinate r. This variable transmission distance is the range curvature,

$$R(a; r) = (r^2 + a^2)^{1/2}, \tag{1a}$$

defined relative to CCRS scene coordinates,[11] or

$$R(\tau; r) = (r^2 + V^2\tau^2)^{1/2}, \tag{1b}$$

relative to DLR remote sensor position and time.[12] The concept of range migration

$$\Delta R(a; r) = R(a; r) - r = (r^2 + a^2)^{1/2} - r \approx a^2/2r, \tag{2}$$

is also illustrated in Fig. 2, where the approximation indicates a binomial expansion[15] of Eq. 1a. This binomial expansion is a good approximation (i.e., $VT/r_0 << 1$ rad)[13] for most SAR systems that obtain enough pulses for a sufficient azimuth history with aperture synthesis times on the order of $T = 1$ s. The minimum range r_0 is the distance of closest approach at the near range edge of the swath occurring at the stationary point in time τ_0. For orbiting SAR platforms, the curvature of the azimuth

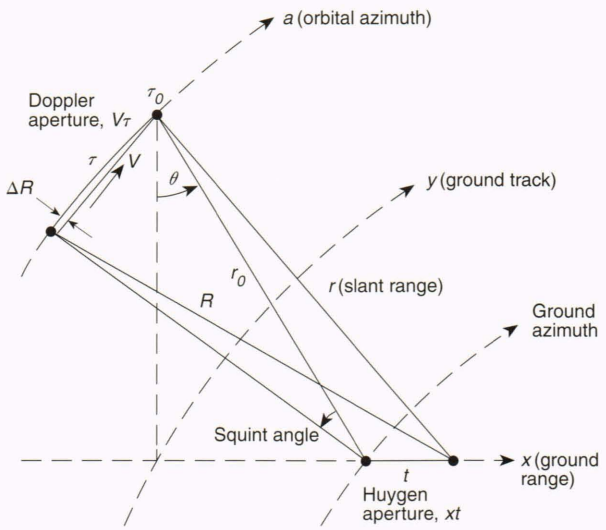

Figure 2. Synthetic aperture radar is an active microwave radar that must transmit in the forward direction so as to receive backscatter with a side-looking geometry. Each successive pulse arriving at a point target has traveled a distance R greater than the slant range r by the differential distance ΔR. This range migration depends on the distance $a = V\tau$ along the Doppler aperture traveled by the remote sensor between transmission and reception of the pulse. (θ = look angle, V = platform velocity, t = short time interval, τ = long time interval, τ_0 = stationary point in time, and r_0 = minimum range.)

coordinates along track must also be considered, since the spacecraft velocity and the ground-track velocity are not equal.

The novel aspect of the CCRS and DLR wave domain processors is the chirp scaling method for equalizing range migration ΔR before data compression. The object is to introduce a phase shift proportional to ΔR at each range time t that will simulate transmission of all pulses from an arbitrary reference range R_{ref}, possibly chosen equal to r_0, but definitely dependent on the differential Doppler time $\Delta\tau = (\tau - \tau_0)$ and its associated Doppler frequency f_a. For a linear frequency-modulated chirp that is phase-locked to range time, this phase shift can be introduced by scaling the chirp rate α with a factor that depends on the Doppler frequency. The new chirp rate,

$$\alpha'(\omega_a) = [(1 - \omega_a^2/4k^2)^{-1/2} - 1]\alpha \ , \qquad (3a)$$

can be formulated with respect to the azimuth wavenumber ω_a of the CCRS scene[11] or the Doppler frequency of the DLR remotely sensed signal,[12]

$$\alpha'(f_a) = [(1 - \lambda^2 f_a^2/4V^2)^{-1/2} - 1]\alpha \ , \qquad (3b)$$

where the quantities in square brackets are the chirp scale factors, C. These quantities are seen to be equivalent using the definitions of the azimuth frequency, $f_a = 1/\Delta\tau$, and azimuth wavenumber

$$\omega_a = 2\pi/\Delta a = 2\pi/V\Delta\tau = 2\pi f_a/V \ , \qquad (4)$$

based on the azimuth space and time coordinate relationship, $a = V\tau$, and the relationship between the radar wavelength λ and the radar wavenumber $k = 2\pi/\lambda$.

The chirp scaling correction for the range migration is made in the range-Doppler domain (t, f_a) and acts on the linear frequency-modulated signal before pulse compression. After pulse compression into the slant range and Doppler wavenumber coordinates (r, ω_a), the result is a complex (i.e., $j = \sqrt{-1}$) signal phase shift,[11]

$$\Delta\Phi = \exp[-j\alpha'(\omega_a)(r - R_{ref})^2] \ , \qquad (5)$$

which also depends indirectly on the radar wavenumber via the scale factor applied to the original chirp rate. The benefit of eliminating range migration is that Doppler compression can proceed toward geometrically correct images without Stolt interpolation[16] and without secondary range compression,[17] although the latter technique might still be used to improve image resolution.

Data Processing Sequence

The chirp scaling correction must precede range compression, since the phase shift that sets the range migration equal to zero is single-valued in the range time and azimuth (i.e., along-track Doppler) frequency domain. Therefore, the azimuth Fourier transform of the signal (over the long time scale associated with the Doppler aperture in space) must be done before computation of the range Fourier transform (over the short time duration of radar pulses). The CCRS and DLR both define a seven-stage SAR imaging process using fast Fourier transform (FFT) methods for applying a complex matched filter to resolve slant range and azimuth image coordinates from raw signal data (see wave domain processing block in Fig. 1). The seven image processing steps are interpreted below for the purpose of describing our Fourier wave filtering processes.

Step 1. Forward FFT in Azimuth

The complex signal to be processed is assumed to have been adequately sampled, including the entire bandwidth of the chirped radar waveform. The modulation of the carrier (C band for ERS-1) is assumed to be down-shifted to a baseband representation. The SAR signal S (Tilley[3]),

$$\begin{aligned} S(\tau, t) &= g(r_0)\int A[x(t), \tau]\exp[jk\{R(t, \tau) + r\}]\, dr \\ &\approx \int A(\tau, t; r)\exp[j\Phi(\tau, t; r)]\, dr, \end{aligned} \qquad (6)$$

transmitted at time τ and received at the stationary point r_0 in space at time τ_0 can be represented in complex notation as a Fresnel–Kirchkoff integral of a complex scattering amplitude A with phase Φ, changing over the Huygen aperture along the ground coordinate $x(t)$. The DLR point response function,[12]

$$\begin{aligned} h(\tau, t; r) &= \exp[j\Phi(\tau, t; r)] \\ &= \exp[-2jkR(\tau; r)] \\ &\quad \times \exp[j\pi\alpha\{t - 2R(\tau; r)/c\}^2], \end{aligned} \qquad (7)$$

neglects the geometry factor, antenna pattern, and pulse envelope, which can be applied as real-valued corrections $g(r_0)$ to the SAR image after aperture synthesis. The time required for the radar signal to travel to the ground and back over the path R is $2R/c$, where c is the speed of light. The first step in both the CCRS and DLR wave domain processes is to take the forward azimuth FFT of the signal $\mathcal{S}$,

$$\mathcal{S}(f_a, t) = \Sigma_\tau S(\tau, t)\exp[-jf_a\tau]\Delta\tau \ , \qquad (8)$$

over the azimuth time coordinate τ.

The following steps create a SAR image of terrain reflectivity. The CCRS radar return from an isolated point scatterer s (Raney[11]),

$$\begin{aligned} s(a, r) &= A[\tau(a), t(r); R(a, r)] \\ &= A[r - R(a), a]\exp[-2jkR(a)] \\ &\quad \times \exp[-j\alpha\{r - R(a)\}^2], \end{aligned} \qquad (9)$$

employs a quadratic phase shift $\exp[-j\alpha\{r - R(a)\}]^2$ for a spherical wavefront $\exp[-2jkR]$ propagating out and back over the path length, which is similar to the exponentials in Eq. 7 for the signal time delay over twice the range curvature.

Step 2. Chirp Scaling

The range migration ΔR can be compensated by multiplying the transform signal $\mathcal{S}(f_a, t)$ by a phase function,

$$\Phi_1(f_a,t;t_{ref}) = \exp\left[j\pi\alpha'(f_a)\left\{\left(1-\frac{\lambda^2 f_a^{\,2}}{4V^2}\right)^{-1/2}-1\right\}(t-t_{ref})^2\right], \quad (10)$$

where the reference time,[12]

$$t_{ref}(f_a) = (2R_{ref}/c)(1 - \lambda^2 f_a^2/4V^2)^{-1/2}, \quad (11)$$

depends indirectly on the reference range R_{ref} and the Doppler frequency via the chirp scale factor,

$$C(f_a) = (1 - \lambda^2 f_a^2/4V^2)^{-1/2} - 1, \quad (12)$$

which is a quadratic function as shown in Fig. 3a. The phase function introduces a first order perturbation,

$$\Delta\Phi(f_a, t) = \exp[j\pi\alpha'(f_a)\,(t - t_{ref})^2] = \exp[j\pi C(f_a)\alpha(t - t_{ref})^2], \quad (13)$$

of the chirp rate α. The phase function Φ_1 is plotted in Fig. 3b as a function of Doppler frequency using parameters appropriate for the ERS-1 SAR.

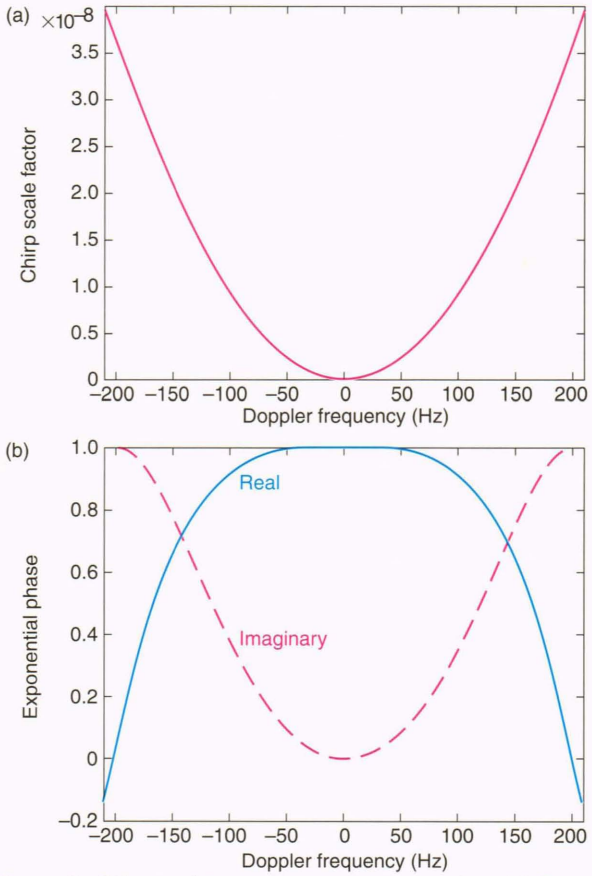

Figure 3. Chirp scaling to correct range migration: (a) Range migration function; (b) phase perturbation function. The correction employs a quadratic factor that shifts the SAR signal phase as a function of Doppler frequency, simulating a circular aperture with all pulses transmitted an equal distance from targets at the reference range. The value of the reference range is arbitrary, but it must be expressed as a function of the Doppler frequency to apply to all points along track that are illuminated by a physical beam which is broad in that direction.

Cumming, Wong, and Raney[18] imply that this phase shift sets all range curvatures equal to that which exists at an arbitrary range R_{ref}. This equalized range curvature can later be eliminated with a two-dimensional phase function that operates in the range and azimuth wavenumber domain (i.e., wave domain). The approach taken in our APL research is to use Eq. 11 for a Doppler frequency-dependent representation of the range reference time, to choose R_{ref} arbitrarily where it appears in Eq. 11, and then to use this R_{ref} consistently in each of the following processing steps.

Step 3. Forward FFT in Range

The third step in both the CCRS and DLR wave domain processes is to take the forward FFT over the range time coordinate t of the range-Doppler domain product of the signal $\mathcal{S}$ and the range migration phasor Φ_1 to yield the SAR signal transform,

$$\mathcal{S}(f_a, f_r; R_{ref}) = \Sigma_t \mathcal{S}(f_a, t)\Phi_1(f_a, t; t_{ref})\exp[-jf_r t]\Delta t, \quad (14)$$

in the two-dimensional wave domain (f_a, f_r) subject to the arbitrary choice of the reference range. In this domain, DLR proceeds with a two-dimensional focusing operation; CCRS is content to focus on range compression with curvature compensation, delaying azimuth focusing to a later stage. We follow the latter approach.

Step 4. Range and Azimuth Correction

The linear frequency-modulated chirp with rate α has quadratic variation in time, $\exp[j\pi\alpha t^2]$, for which the appropriate matched compression filter is $\exp[j\pi f_r^2/\alpha]$, the Fourier domain equivalent. Substitution of $a = V\tau$ into Eq. 2 yields a range migration expression whose Fourier domain equivalent enters into the phase function,

$$\Phi_2(f_a, f_r; r_0) = \exp\left[\frac{j\pi(f_r^{\,2}/\alpha)}{C(f_a)} + 1\right] \times \exp\left[j\pi\left\{\left[(f_0 + f_r)^2 - \left(\frac{2f_a}{Vc}\right)^2\right]^{1/2} - f_0 + f_r\right\} \times \frac{c\tau_0(f_a; f_c, r_0)}{2}\right], \quad (15)$$

which is plotted in Fig. 4. The offset frequency f_0 is added to the range coordinate frequency f_r as a change of variable[19] required to obtain the skewed frequency $f_0 + f_r$ along the range curvature R.

The principle of stationary phase[10,13] is used in Eq. 15 to define the signal frequency offset,

$$f_0 = f_c + \alpha\tau_0(f_a; f_c, r_0), \quad (16)$$

from the Doppler center frequency,

$$f_c = 2V_r/\lambda, \quad (17)$$

shifted from zero by the rotational speed V_r of the Earth relative to the remote sensor at the stationary point in time

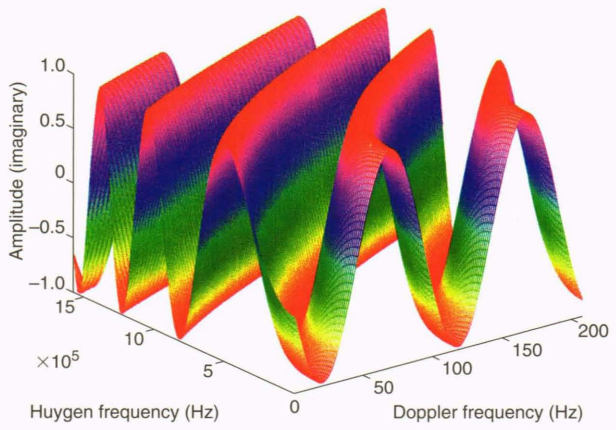

Figure 4. Two-dimensional wave domain compression function. A complex matched filter compresses signal data in the range and azimuth coordinates of the two-dimensional Fourier wavenumber domain. The data compression simulates the simultaneous transmission of all pulses from the many points composing the synthetic Doppler aperture along track and, furthermore, simulates simultaneous transmission of all chirp frequencies within an instantaneous pulse. The effect is that of illuminating the Earth for a moment in time with a large two-dimensional antenna in space.

τ_0. As the transmitted wavefront propagates along the range curvature R with wavenumber, $k = 2\pi/\lambda$, its phase,

$$\phi(\tau) = 2k(r^2 + V^2\tau^2)^{1/2}, \tag{18}$$

oscillates rapidly. However, at the stationary point,[13] the phase rate equals the frequency:

$$\begin{aligned} 2\pi(f_a - f_c) &= -d\phi(\tau)/d\tau = -2V^2k\tau/(r^2 + V^2\tau^2)^{1/2} \\ &\approx -2V^2k\tau_0/r_0, \end{aligned} \tag{19}$$

yielding the expression $\tau_0(f_a; f_c, r_0)$ in Eqs. 15 and 16 for the stationary time in the wavenumber domain. Note that the binomial approximation is not employed. Hence, this wave domain method is fully applicable to wide-swath and high-squint geometries. However, the use of r_0 in the denominator of Eq. 19 assumes that the range curvature is fully compensated before this pulse compression.

Wave domain compression is achieved by applying the principle of stationary phase, yielding a new signal,

$$\mathcal{S}(f_a, f_r; r_0, R_{ref}) = \Phi_2(f_a, f_r; r_0)\mathcal{S}(f_a, f_r; R_{ref}), \tag{20}$$

and focusing the range coordinate.

Suppose the ground track is oriented at angle Ψ from true north at latitude $\mathfrak{L}$ with a look angle θ from the vertical. Then a relative SAR sensor–Earth rotation velocity,

$$V_r = 465\ \cos(\mathfrak{L})\cos(\Psi)\sin(\theta)\ \text{m/s}, \tag{21}$$

can be computed to estimate the Doppler center frequency.[1,20] An important objective of our research is experimentation with such approximations and model parameters to determine an optimum APL wave domain algorithm for accurate compression of SAR scenes.

Step 5. Inverse FFT in Range

The high-frequency components of the signal are redistributed in Eq. 20 to correct for the migration of radar cross section across range cell boundaries. These radar cells are defined after data compression by inverse Fourier transformation over range frequency f_r, yielding the range-Doppler signal,

$$\mathcal{S}(f_a, r; r_0, R_{ref}) = \Sigma_{f_r}\, \mathcal{S}(f_a, f_r; r_0, R_{ref})\exp[jf_r r]\Delta f_r, \tag{22}$$

where the dimension of the range cells is fixed by the product of pulse bandwidth and the pulse duration time over which the forward FFT was computed in Step 3.

Step 6. Azimuth Focusing

The azimuth bandwidth is considered in the second exponential phasor appearing in Eq. 15. Another matched filtering operation is required, however, to focus the azimuth coordinate. Runge and Bamler[12] offer the following phase function to complete azimuth processing:

$$\begin{aligned} &\Phi_3(f_a, r; R_{ref}) \\ &\quad = \exp\left[j\left(\frac{4\pi}{\lambda}\right)\left(\frac{c\tau/2 - R_{ref}}{C(f_a)+1}\right)\right] \\ &\qquad \times \exp\left[-j\alpha\pi C(f_a)\{C(f_a)+1\}\left(\tau - \frac{2R_{ref}}{c}\right)^2\right], \end{aligned} \tag{23}$$

where $\tau = \tau(f_a, r)$ in the range-Doppler domain via solution of the fully quadratic form of Eq. 19. This phase function is then applied to the range-Doppler signal,

$$\mathcal{S}(f_a, r; r_0, R_{ref}) = \Phi_3(f_a, r; R_{ref})\mathcal{S}(f_a, r; r_0, R_{ref}), \tag{24}$$

in the slant range and Doppler frequency domain. This azimuth focus is correct for stationary data with no platform altitude or speed variation. Alternatively, the stationary Doppler center frequency f_c can be computed from a clutterlock analysis[10] of the range-Doppler data. Nonstationary Doppler frequency shifts could enter many of the steps above (e.g., Eqs. 10, 15, 16, and 20). The investigation of nonstationary estimation procedures with experimental error evaluation is likely to be important in the development of low-altitude airborne remote sensor applications.

Step 7. Inverse FFT in Azimuth

The azimuth image coordinate is formed by taking the inverse FFT of the range-Doppler data spectrum. The result is a complex SAR image,

$$s(a, r; r_0, R_{ref}) = \Sigma_{f_a}\mathcal{S}(f_a, r; r_0, R_{ref})\exp[jf_a a]\Delta f_a, \tag{25}$$

in the along-track and slant range coordinates (a, r) subject to the distance of closest approach r_0 and arbitrary reference range R_{ref}. We can detect this complex SAR image by taking its absolute value as a single-look representation of the scene.

An eighth process can be added to this list for interpolation of the slant range image to ground range coordinates. Skewing[21] of the image coordinates often occurs during azimuth focusing with the range-Doppler algorithm. This azimuth skew should be removed (but often is not) during the slant range to ground range resampling of the SAR image,[5,14] given the Doppler focusing parameters, pulse repetition period, and number of incoherent

looks employed during azimuth processing. This geometric skew is directly proportional to the center Doppler frequency. This effect is negligible for the ERS-1 platform that we chose as a test case, since it tracks f_c to compensate for the Earth's rotation. Hence, after detecting the SAR image, the range coordinate was resampled without compensating for any azimuth skew in these early data processing experiments.

Initial Experiments with ERS-1 Satellite Data

An ERS-1 satellite scene of the Chesapeake Bay had been studied at APL for its resolution properties[8] using a multilook detected (MLD) real data format produced by a range-Doppler SAR processor at CCRS. The same scene has since been acquired from CCRS in a complex signal format for use in developing a wave domain SAR processor at APL. These data were recorded by the advanced microwave instrument aboard the ERS-1 satellite on 9 May 1992 during orbit 4257 over the Chesapeake Bay. The MLD data product is adequate for environmental applications; the duplication of the scene with a wave domain processor is desirable for the separate purpose of testing a new SAR imaging algorithm for its accuracy and efficiency. The ability to compare our wave domain SAR processing results with those of an established range-Doppler SAR processor was a secondary objective that is supported by the CCRS data sets.

The raw SAR signal data set consists of complex SAR signal samples, 5 bits in-phase and 5 bits quadrature, in two separate 8-bit formats. These C-band radar data have been converted to baseband but maintain the chirped waveform without range compression of the pulse envelope. A 300-μs window on the return pulse is represented as 5616 samples down range. Approximately 17 s of data along track are represented by 30,000 returns from terrain illuminated with a pulse repetition frequency of 1680 Hz. A computer program was developed in the Matlab language to process SAR signal data using generic radar and platform parameters (e.g., the ERS-1 values listed in Table 1) to create images of littoral scenes.

Table 1. Matlab parameters for ERS-1 synthetic aperture radar image processing.

Parameter	Value
Radar	
Pulse bandwidth	15.5 MHz
Radar wavelength	5.656 cm
Pulse repetition frequency	1679.9 Hz
Pulse duration time	37.1 μs
Sampling frequency	18.96 MHz
Doppler bandwidth	1183 Hz
Platform	
Platform velocity	6700 m/s
Platform altitude	780 km
Near-edge incidence angle	19.376°
Direction relative to north	15°
Latitude of scene	35°
Radius of Earth	6400 km

The main Matlab program defines global variables and controls the sequential flow of SAR data in calling three major Matlab subprograms (migration, compression, and detection). The migration procedure computes a forward Fourier transformation of the azimuth coordinate and applies a Doppler frequency-dependent chirp scale factor as a Fourier phase perturbation to compensate for range curvature. The compression procedure applies a two-dimensional Fourier wavenumber domain filter for range focusing and compression of the central Doppler band. The detection procedure includes azimuth focusing and an inverse Fourier transformation before detecting the amplitude of the complex SAR single-look image.

Our wave domain method involved an arbitrary choice of the reference range R_{ref} for chirp scaling to eliminate range migration. A SAR processing strategy was defined to apply these Matlab procedures to 48 subswaths down range, each containing 117 range cells, wherein the range migration and compression filter parameters were based on a stationary reference range chosen at the far edge of each subswath. For each of the 48 range blocks, 4096 azimuth pulse returns detecting one azimuth strip were input to a 64-bit complex data buffer constrained by Matlab memory limitations. The Doppler bandwidth was later reduced from 4096 to 1024 pulses (pre-summing the azimuth coordinate by a factor of 4) to save processing time for each of 7 azimuth strips. A corner turn of the raw data (that is, a matrix transposition of a $1024 \times 117 \times 64$ bit array of complex SAR data) was required to accomplish chirp scaling in the Doppler frequency domain before pulse compression of the entire swath down range. After pulse compression in the two-dimensional wave domain, a second corner turn was required to accommodate single-look detection of 8-bit SAR scattering intensities defined as absolute magnitudes of the complex data.

The spatial resolution of the APL wave domain process was demonstrated by processing a single azimuth strip after choosing a data segment down range that included the bridge across the Chesapeake Bay at Kent Island. Doppler frequency analysis of the raw data was performed at CCRS and used at APL to define an optimal azimuth focus for this strip. A Doppler frequency rate of 2155 Hz/s was used for azimuth focusing (Step 6), replacing the estimate of 1912 Hz/s provided by Eq. 19. Two looks were computed and averaged by taking both roots in computing $\tau(f_a; f_c, r_0)$. Azimuth compression (Step 4) benefited from the CCRS estimates of the Doppler frequency rate and the Doppler center frequency, with 301 Hz replacing the 530 Hz estimated via Eq. 17. This Chesapeake scene was then combined with earlier Seasat SAR and Landsat thematic mapper (TM) infrared scenes of the Bay Bridge. A color composite is depicted in Fig. 5 with the Seasat SAR represented in red, Landsat TM in green, and our APL-processed ERS-1 SAR scene in blue. The geometric registration of the two SAR scenes can be evaluated by observing that the hues involving the green Landsat TM database change abruptly along the coastlines of the bay. The individual satellite scenes are also shown in Fig. 5, interpolated to a common 25-m spatial grid.

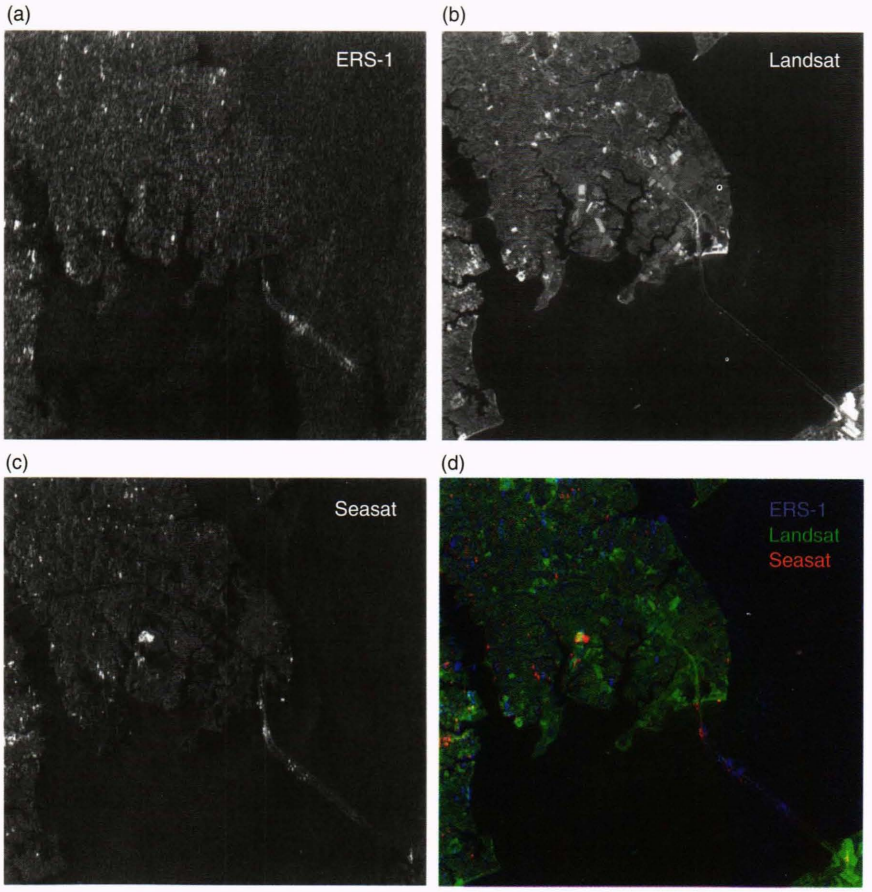

Figure 5. (a) The APL-processed ERS-1 SAR scene of the two spans of a bridge across the Chesapeake Bay is compared at 25-m resolution with similar scenes. (b) The Landsat-4 thematic mapper (TM) infrared image. (c) Seasat SAR remote sensor. (d) The color composite represents the Seasat SAR scene in red, the Landsat TM scene in green, and our APL-processed ERS-1 SAR scene in blue. (Data from ERS-1; reprinted by permission of the European Space Agency.)

For a larger scene of the Chesapeake region, both the range and the azimuth coordinates were averaged in 8×8 blocks of picture elements. Hence, our APL-processed ERS-1 Chesapeake Bay scene, depicted in Fig. 6, consisted of 48×7 blocks of data, each subjected to Matlab wave domain algorithms requiring two corner turns of two 117×1024 arrays (both in-phase and quadrature) of 32-bit Matlab floating point data. The 48 range subswath boundaries were not a problem in the APL wave domain process, since the full beamwidth was available for the down-range FFTs. However, some of the seven azimuth strip boundaries are apparent near the center of the scene (Fig. 6a). Geometric shapes are continuous across these strip boundaries along track, but radiometric detection is compromised by the limited size of the azimuth transform. The CCRS-processed ERS-1 Chesapeake Bay scene shown in Fig. 6b has better radiometric properties as the result of detection and averaging of six looks. Both scenes have been resampled to a grid matching the resolution of our Kodak Model 77 printer. The 125-m picture elements demonstrate the geometric accuracy of the APL wave domain process, which has included slant range to ground range conversion of the image perspective.[1]

The ERS-1 satellite orbited at an altitude of 780 km and covered a 100-km swath (e.g., 98 km in Fig. 6a and 108 km in Fig. 6b). A Russian satellite (Almaz) and the Japanese Earth Resources Satellite (JERS-1) have also recently recorded Chesapeake Bay scenes, shown in Figs. 6c and 6d, respectively, for comparison. The Almaz SAR was orbited at 280 km and covered a 40-km swath. The JERS-1 image was created at the Remote Sensing Technology Center of Japan using a range-Doppler algorithm to synthesize a 75-km SAR swath from data remotely sensed at an altitude of 570 km.

REMOTE SENSING OF AIR–SEA INTERACTIONS

A surface analysis of the Chesapeake region for the morning of 9 May 1992 indicated the convergence along the East Coast of a warm front and a cold front advancing toward the north and curving toward the west (Fig. 7). Rainfall was reported on surface weather maps for the 24-h periods before and after 7:00 a.m. on 9 May 1992 (weekly series, 4–10 May, of daily weather maps from the Climate Analysis Center, NOAA). A westward 10-kt (i.e., 5-m/s) wind was blowing inland to the north of the cold front associated with a low-pressure system located over Ohio. Surface winds were calm in the cooler air mass south of the frontal zone, except for a 10-kt breeze blowing up along the coast, where dew points were within a few degrees of air temperature. The ERS-1 SAR image, shown in Fig. 6, was recorded at 3:20 a.m., at which time the cold front was very near the Bay Bridge at Kent Island. The upper bay has been roughened by the wind to the extent that the mean SAR backscatter is nearly as strong as that of land observed along the western shore.

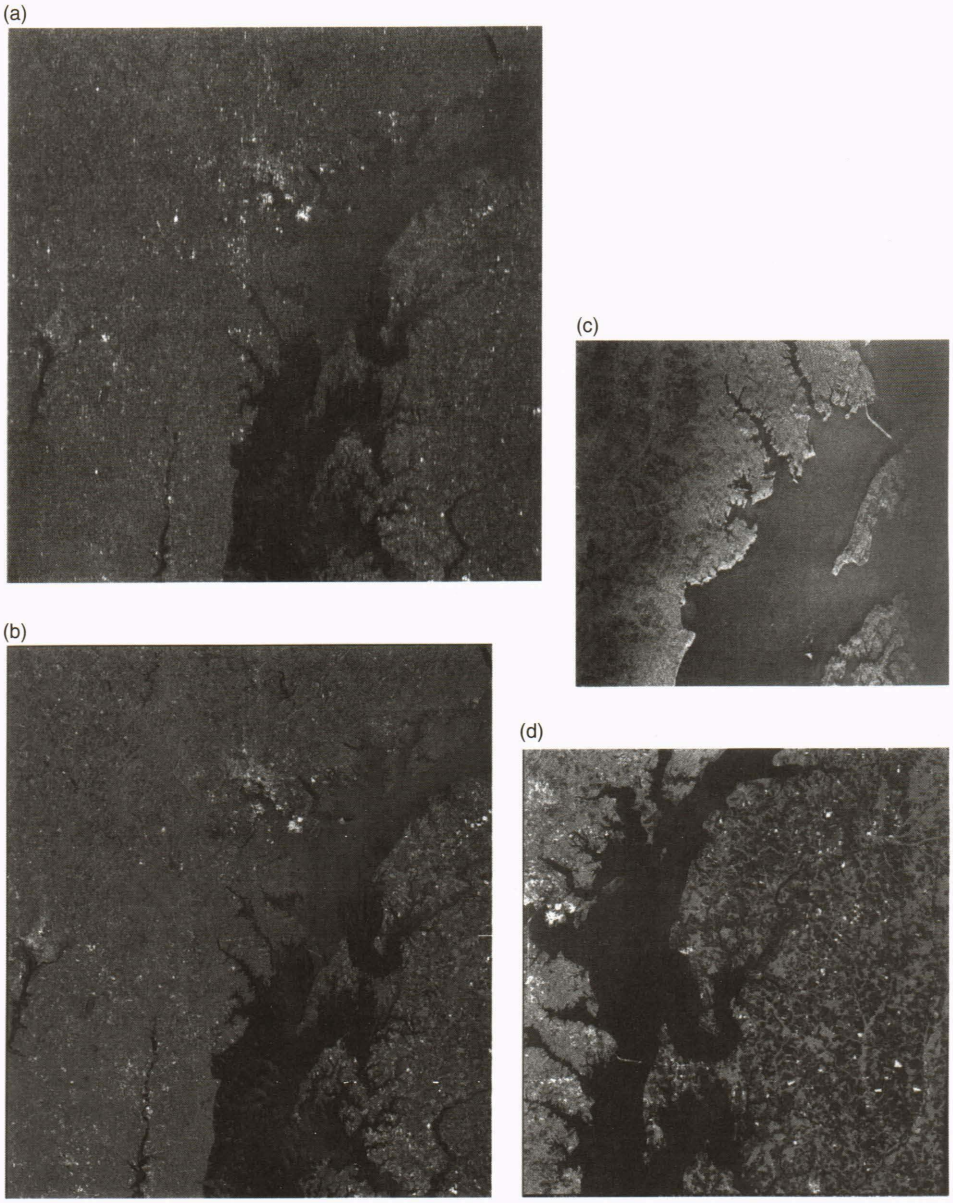

Figure 6. The ERS-1 SAR scene of the Chesapeake Bay for 9 May 1992, created with (a) the APL wave domain process and (b) the CCRS range-Doppler process. (c) The Almaz SAR scene for 22 May 1991 created in Moscow at NPO Mashinostroenia. (d) The Japanese Earth Resources Satellite (JERS-1) SAR scene for 6 July 1993 created at the Remote Sensing Technology Center in Japan.

The lower bay is almost completely dark in the SAR image except for several parallel striations separated by 3–4 km. Hence, the smooth, sheltered waters of the Chesapeake Bay provide a canvas upon which nature has clearly pictured the signature of an air–sea interaction.

The same morning, an AVHRR remote sensor aboard a NOAA satellite also photographed nature's effect on these coastal waters. At 8:52 a.m., 5.5 h after the ERS-1 SAR overpass, the AVHRR channel 4 radiometer recorded the scene shown in Fig. 8. This thermal infrared wavelength (10.4–11.4 μm) is generally used to indicate sea surface temperature when the surface is not obscured by clouds. However, in this case the clouds are of interest because there seem to be both cold clouds and, presumably at a lower altitude, warmer clouds. The cold cumulus clouds are depicted in white and the warmer stratiform clouds in black. On the basis of reported dew points, the black clouds were determined to be moisture laden and much closer to the water surface. The most notable of these dark clouds is a plumelike pattern beginning in the lower left corner as a dense and narrow flow that appears to rise, cool, and disperse as it approaches the center of the scene. This filamentary river in the sky[22] also appears to be associated with a warmer region spreading out over the water surface below the plume. This may be an AVHRR signature of rainfall. The Gulf Stream south of Cape Hatteras is depicted in dark blue and seems to be the source of the moisture-laden air. Earlier, when the

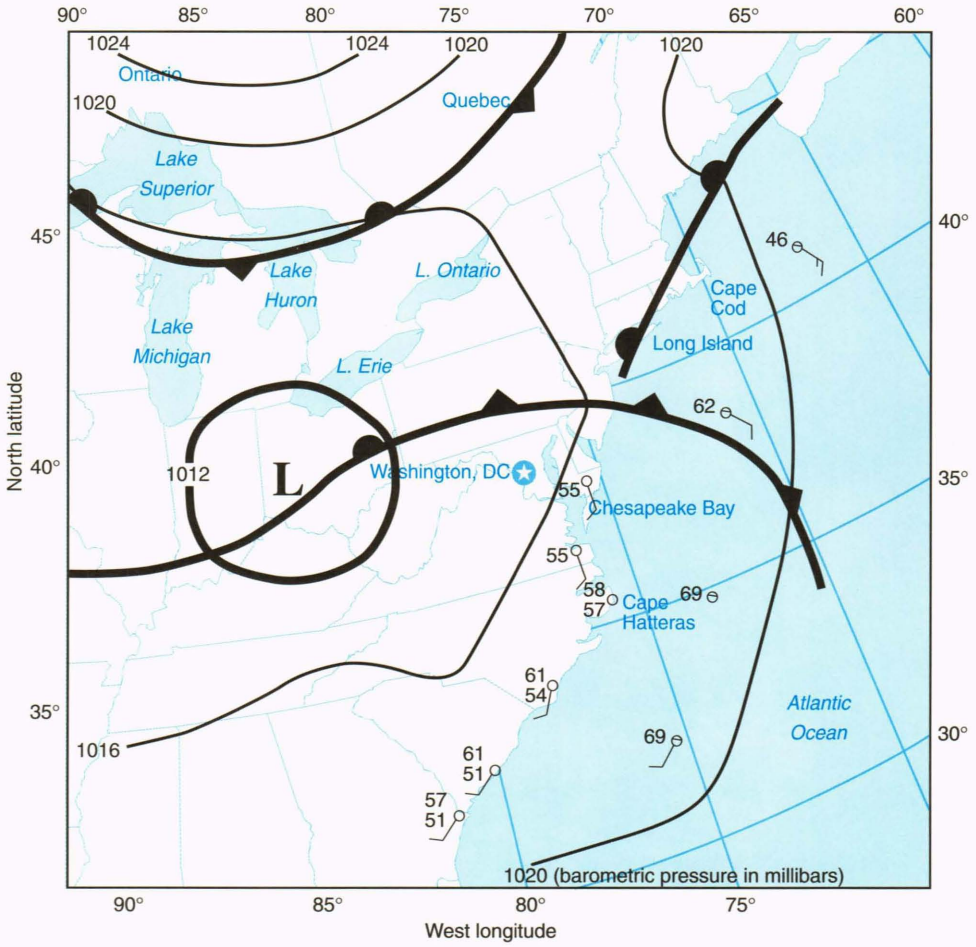

Figure 7. A surface weather map of the eastern United States depicts a low-pressure system over the Ohio Valley and an associated cold front advancing northward. The warm front moving westward also is associated with the counterclockwise circulation around the low-pressure system. Rainfall was also reported for the Chesapeake region for 8–10 May 1992.

SAR passed over the region at 3:20 a.m., this flow of moist air may have been undulating over the bay to roughen its surface in the pattern of an atmospheric wave, much like oceanic internal waves[23] that propagate in the boundary layer beneath the surface.

The AVHRR cloud scene also indicates the presence of atmospheric roll vortices and wind rows,[24] which were created by the convergence of Langmuir cells in the surface boundary layer. These cloud formations are generated parallel to strong winds like those that were blowing inland along the frontal boundary. The AVHRR striations in the upper left corner of Fig. 8 are separated by about 5 km, comparable to the separation of the SAR striations observed in Fig. 6. Roll vortices are observed by sailors as increases in the surface wind stress caused by convergence of vertical flows in front of an advancing air mass. Hence, surface expressions of these AVHRR cloud features could account for the atmospheric signature found in the SAR image earlier and farther south.

CONCLUSIONS

A new SAR imaging algorithm was used to synthesize an ERS-1 satellite scene of the Chesapeake Bay. Wave domain processes were implemented with a Matlab program running on a Hewlett-Packard workstation without any parallel processor in support. The geometric accuracy of the chirp scaling method was demonstrated by comparisons of our APL single-look SAR image with a multilook SAR image produced at CCRS and with an earlier Landsat scene of the bay. The form and function of the chirp scaling algorithms and the two-dimensional wave domain filters were demonstrated for 48 sub-beams forming a continuous 100-km swath down range and 7 strips along track. The azimuth strips were contiguous geometrically, although the radiometrics were not continuous across the seams. A large speckle noise component and suboptimum azimuth resolution are the result of the narrowband single-look process. The block averaging of return pulses, or pre-summing the azimuth coordinate, also results in suboptimal resolution.

Future work should include the development of improved processing methods. Methods for secondary range compression and azimuth focusing should be developed in conjunction with signal data that are neither pre-summed nor segmented in azimuth. Additional programming is required to accomplish multilook processing using several Doppler frequency bands to match sensor resolution and reduce speckle noise. Radiometric

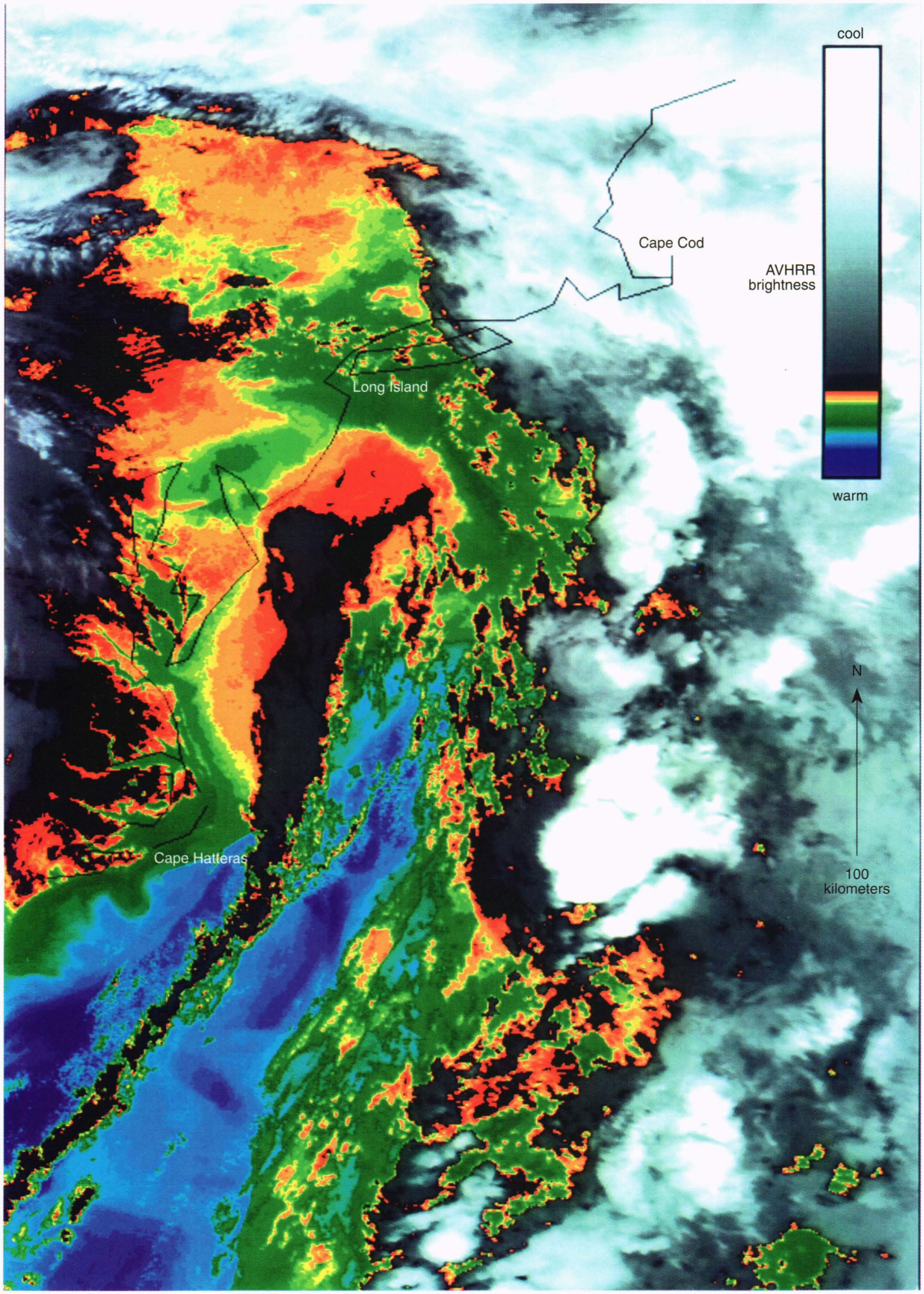

Figure 8. An AVHRR infrared scene of clouds over the East Coast of the United States was recorded by a NOAA satellite on the morning of 9 May 1992. The riverlike feature extending from the lower left may be the signature of atmospheric moisture flowing northward above the Gulf Stream; this moisture precipitates as rainfall near the center of the scene.

corrections for the pulse power envelope, scattering angle, and antenna pattern down range should be developed to represent the SAR image in units of radar cross section.

Clutterlock methods for estimating the center Doppler frequency in the azimuth focusing stage could be used to develop nonstationary Fourier filtering methods for dealing with variations in altitude, speed, and squint angle. These unknown attitude variations probably account for the large discrepancy in the Doppler center frequencies (for example, 530 Hz as compared with 301 Hz) computed from orbit parameters and estimated from raw data. The smaller discrepancy in the computed and estimated Doppler frequency rates (for example, 1912 Hz/s as compared with 2155 Hz/s) probably results from the imprecise specification of platform velocity parameters. The use of better ancillary information, including platform attitude, chirp replicas, and range gate timing, should be investigated for improvements in SAR image resolution. The stationary phase principle should be reconsidered for high-altitude orbital geometries where azimuth curvature, as well as range curvature, is significant. As these issues are resolved for the ERS-1 satellite, we will have a standard SAR process for data from the ERS-2 satellite to be launched in 1996. We also will be in a good position to develop a value-added SAR process for data from Radarsat, which will be launched next year. Future developments in SAR processing capabilities will be guided by a consensus opinion on chirp scaling methods.[25]

The APL wave domain processor was developed under the APL Independent Research and Development Program to support the performance analysis of generic SAR systems. The Virtual SAR Project now provides a capability for analyzing scene distortions caused by geometric approximations in the digital imaging algorithms. The side-looking binomial approximation required by the range-Doppler algorithm is not essential to the wave domain algorithm. Forward-looking aircraft SAR applications and wide-swath interferometric SAR applications that require large squint angles can be modeled and designed using wave domain SAR processing algorithms. Sensing vehicle speeds on highways or measuring terrain topography from aircraft may be possible. SAR data from aircraft should be analyzed to generate categorical descriptions of littoral terrain. The simulation of terrain as sensed by remote radar systems has been made feasible by recent advances in computer technology. Future enhancements of the radar terrain simulator will provide control over the raw signal data input to our SAR image processor. A single computer model will enable performance studies for a variety of littoral terrain categories and SAR system designs.

REFERENCES

[1] Tilley, D. G., and Bonwit, K. S., "Reduction of Layover Distortion in SAR Imagery," *Remote Sens. Environ.* **27**, 211–220 (1989).

[2] Jenkins, J. O., Randolph, J. P., Tilley, D. G., and Waters, C. A., "The APL Image Processing Laboratory," *Johns Hopkins APL Tech. Dig.* **5**(1), 59–78 (1984).

[3] Tilley, D. G., "Use of Speckle for Determining the Response Characteristics of Doppler Imaging Radars," *Opt. Eng.* **25**(6), 772–779 (1986).

[4] Tilley, D. G., "Amplitude Distributions for Seasat SAR and Skylab Data with Statistics for Classification and Correlation," *Electromagnetics* **4**, 297–308 (1984).

[5] Tilley, D. G., and Beal, R. C., "ERS-1 and Almaz SAR Ocean Wave Imaging over the Gulf Stream and Grand Banks," in *Proc. First ERS-1 Symp.: Space at the Service of our Environment*, ESA SP-359, pp. 729–734, Cannes, France (Nov 1992).

[6] O'Keefe, S., Kelso II, F. B., and Mundy, C. E., "...From the Sea, Preparing the Naval Service for the 21st Century," *NavNews* 046/92, Navy News Service (Sep 1992).

[7] Evers, S., "GNAT-750 May Raise Profile of UAVs," *Aviat. Week Space Technol.*, 54–55 (Feb 1994).

[8] Tilley, D. G., and Beal, R. C., "ERS-1 and Almaz Estimates of Directional Ocean Wave Spectra Conditioned by Simultaneous Aircraft SAR and Buoy Measurements," *Atmos.–Ocean* **32**(1), 113–142 (1994).

[9] Beal, R., Kudryavtsev, V., Thompson, D., Grodsky, S., Tilley D., and Doluv, V., "Large and Small Scale Circulation Signatures of the ERS-1 SAR over the Gulf Stream," in *Proc. Second ERS-1 Symp.: Space at the Service of our Environment*, ESA SP-361, pp. 547–551, Hamburg, Germany (Oct 1993).

[10] Curlander, J. C., and McDonough, R. N., *Synthetic Aperture Radar Systems and Signal Processing*, John Wiley and Sons, New York, pp. 142–144, 154–209, 224–226 (1991).

[11] Raney, R. K., "An Exact Wide Field Digital Imaging Algorithm," *Int. J. Remote Sens.* **13**(5), 991–998 (1992).

[12] Runge, H., and Bamler, R., "A Novel High Precision SAR Focussing Algorithm Based on Chirp Scaling," in *Proc. Int. Geosci. Remote Sens. Symp. I*, pp. 372–375 (May 1992).

[13] Harger, R. O., *Synthetic Aperture Radar Systems Theory and Design*, Academic Press, New York, pp. 20, 55–57 (1970).

[14] McDonough, R. N., Raff, B. E., and Kerr, J. L., "Image Formation from Spaceborne Synthetic Aperture Radar Signals," *Johns Hopkins APL Tech. Dig.* **6**(4), 300–312 (1985).

[15] Bamler, R., "A Systematic Comparison of SAR Focussing Algorithms," in *Proc. Int. Geosci. Remote Sens. Symp. II*, pp. 1005–1009 (Jun 1991).

[16] Monti-Guarnieri, A., Prati, C., and Rocca, F., "SAR Focusing in Non-Standard Geometries: A Generalized Approach," in *Proc. Int. Geosci. Remote Sens. Symp. I*, pp. 369–371 (May 1992).

[17] Chang, C. Y., Jin, M. Y., and Curlander, J. C., "SAR Processing Based on the Exact Two-Dimensional Transfer Function," in *Proc. Int. Geosci. Remote Sens. Symp. I*, pp. 355–359 (May 1992).

[18] Cumming, I., Wong, F., and Raney, K., "A SAR Processing Algorithm with No Interpolation," in *Proc. Int. Geosci. Remote Sens. Symp. I*, pp. 376–379 (May 1992).

[19] Cafforio, C., Prati, C., and Rocca, F., "SAR Data Focusing Using Seismic Migration Techniques," *IEEE Trans. Aerosp. Electron. Syst.* **27**(2), 194–207 (1991).

[20] Tilley, D. G., Kerr, J. L., and Vogt, C. L., "The Influence of Platform Attitude on the Doppler Frequency Synthesis of SIR-B Ocean Data Near Hurricane Josephine," in *Proc. IGARSS'89: Quant. Remote Sens. 4*, pp. 2696–2699 (Jul 1989).

[21] Curlander, J. C., and Pang, S. N., "Geometric Registration and Rectification of Spaceborne SAR Imagery," in *Proc. Int. Geosci. Remote Sens. Symp. II(Fa 2)*, pp. 5.5–5.6 (1982).

[22] Newell, R. E., Newell, N. E., Zhu, Y., and Scott, C., "Tropospheric Rivers—A Pilot Study," *Geophys. Res. Lett.* **12**(24), 2401–2404 (1992).

[23] Apel, J. R., Thompson, D. R., Tilley, D. G., and Van Dyke, P., "Hydrodynamics and Radar Signatures of Internal Solitons in the Andaman Sea," *Johns Hopkins APL Tech. Dig.* **6**(4), 330–337 (1985).

[24] Hanson, J. L., "Winds, Waves, and Bubbles at the Air–Sea Boundary," *Johns Hopkins APL Tech. Dig.* **14**(3), 200–208 (1993).

[25] Raney, R. K., Runge, H., Bamber, R., Cumming, I., and Wong, F., "Precision SAR Processing Using Chirp Scaling," *IEEE Trans. Geosci. Remote Sens.* **32**(4), 786–799 (1994).

ACKNOWLEDGMENTS: The authors appreciate the time and experience contributed by the APL staff in the review and editing of this article. Surface weather maps were provided by Julius Goldhirsh, and Steve Babin joined in discussing them. We discussed Doppler frequency characteristics for the ERS-1 signal data with Julian Prinz at the Canada Centre for Remote Sensing. The efficient management of the ERS-1 satellite and its ground processing stations by the European Space Agency is also recognized and appreciated.

THE AUTHORS

DAVID G. TILLEY received a B.S. degree in physics from the University of Virginia in 1969. In 1970 and 1971 he served at the VII Corps Headquarters while in the U.S. Army Signal Corps. He earned a Ph.D. degree in nuclear engineering in 1976 and an M.S. degree in electrical engineering in 1979, both from The Pennsylvania State University. Dr. Tilley joined the Computing Branch at APL in 1979 and moved to the Space Department in 1986, where he has been co-investigator for ocean science with satellite and shuttle imaging radars. He is currently co-investigator for the Virtual SAR Project in the Independent Research and Development Program. Other research interests are radar statistics and atmospheric physics.

DAVID J. YEMC received a Bachelor of Electrical Engineering degree (cum laude) in 1983 from the University of Delaware. He attended the Rensselaer Polytechnic Institute as a Raytheon Company Miccioli Scholar and earned a Master of Electrical Engineering degree in 1985. In 1990, after employment with the Raytheon Company and with E-Systems, Inc., he joined the Senior Staff of APL. Mr. Yemc has worked on adaptive array processing for radar systems during the past 10 years and was the principal investigator for a diversely polarized array antenna project. He is currently co-investigator for the Virtual SAR Project in the Independent Research and Development Program.